

Multimodal Deep Learning for Phyllodes Tumor Classification from Ultrasound and Clinical Data

Farhan Fuad Abir¹, Abigail Elliott Daly³, Kyle Anderman³, Tolga Ozmen³, and Laura J. Brattain²

¹Department of Electrical and Computer Engineering, University of Central Florida, Orlando, FL, USA

²Department of Internal Medicine, University of Central Florida College of Medicine, Orlando, FL, USA

³Massachusetts General Hospital, Department of Surgery, Section of Breast Surgery, MA, USA

Abstract—Phyllodes tumors (PTs) are rare fibroepithelial breast lesions that are difficult to classify preoperatively due to their radiological similarity to benign fibroadenomas. This often leads to unnecessary surgical excisions. To address this, we propose a multimodal deep learning framework that integrates breast ultrasound (BUS) images with structured clinical data to improve diagnostic accuracy. We developed a dual-branch neural network that extracts and fuses features from ultrasound images and patient metadata from 81 subjects with confirmed PTs. Class-aware sampling and subject-stratified 5-fold cross-validation were applied to prevent class imbalance and data leakage. The results show that our proposed multimodal method outperforms unimodal baselines in classifying benign versus borderline/malignant PTs. Among six image encoders, ConvNeXt and ResNet18 achieved the best performance in the multimodal setting, with AUC-ROC scores of 0.9427 and 0.9349, and F1-scores of 0.6720 and 0.7294, respectively. This study demonstrates the potential of multimodal AI to serve as a non-invasive diagnostic tool, reducing unnecessary biopsies and improving clinical decision-making in breast tumor management.

Index Terms—phyllodes tumor, breast ultrasound, multimodal AI, feature fusion, class-aware sampling

I. INTRODUCTION

Breast fibroepithelial lesions are a diverse group of biphasic tumors consisting of fibroadenomas (FAs) and phyllodes tumors (PTs). While FAs are common benign tumors with a low risk of recurrence or metastasis, PTs are rare lesions, accounting for less than 1% of breast tumors, that exhibit heterogeneous characteristics [1]. However, their clinical significance lies in the uncertain progression and the diagnostic challenges [2]. Moreover, the World Health Organization (WHO) classifies phyllodes tumors into benign, borderline, and malignant subtypes with reported local recurrence rates of 7.1%, 16.7%, and 25.1%, respectively [3]. Therefore, accurate preoperative grading of PTs into benign versus borderline/malignant is crucial for appropriate treatment planning.

The current standard diagnostic pathway often involves a core needle biopsy (CNB), followed by surgical excision if pathology is ambiguous. However, up to 57% of CNB-diagnosed fibroepithelial lesions are later upgraded to phyllodes tumors after excision, leading to unnecessary surgeries with potential complications, scarring, and increased health-care costs. In the United States alone, excisional biopsies for suspected phyllodes tumors cost over \$2 million annually [1],

[4]. Artificial Intelligence (AI) offers a promising solution in this regard.

Early efforts focused on ultrasound (US) imaging alone. Yan et al. developed a deep learning (DL) model differentiating PTs from fibroadenomas (FAs) with 87.3% accuracy using multicenter ultrasound data [3]. Similarly, the Xception architecture achieved an AUC of 0.87 for PT-FA discrimination [5]. However, these models lacked clinical context, limiting their diagnostic utility in ambiguous cases [6].

Multimodal AI approaches often integrate imaging with structured clinical data and they showed significant promise in broader breast cancer diagnostics. Ben et al. incorporated patient metadata with mammography, which improved molecular subtyping AUC by up to 27.6% over image-only models [7]. Similarly, fusing B-mode ultrasound with Nakagami parametric imaging increased AUC by 10.75% [8], and combining mammography and ultrasound boosted specificity to 96.41% [9]. Xu et al. integrated morphological and texture features which reduced false positives in BI-RADS 4 lesions by 15% [10]. Despite this progress, multimodal strategies have rarely been applied to phyllodes tumors, where models continue to rely on ultrasound or histopathological features in isolation. This is a critical gap, as clinical variables such as age, tumor size, and menopausal status are central to radiologists' real-world assessments and could significantly enhance diagnostic performance in AI models.

In this work, we propose a multimodal deep learning framework that integrates ultrasound imaging with structured clinical data to improve phyllodes tumor classification. Our dual-branch architecture fuses spatial features from ultrasound with patient-level metadata, enabling the model to capture complementary diagnostic cues. We apply class-aware sampling and subject-stratified 5-fold cross-validation to mitigate class imbalance and prevent data leakage. We also evaluated our method on multiple image encoders and outperformed unimodal baselines, highlighting its potential as a non-invasive decision support tool in clinical workflows.

II. METHODS

A. Dataset

The phyllodes tumor dataset was retrospectively collected and anonymized at the Massachusetts General Hospital (MGH). The study was approved by the Institution Review

Board. The deidentified dataset comprises clinical data from 106 subjects, breast ultrasound (BUS) images from 71, and videos from 10 subjects in DICOM format. Not all subjects had complete clinical and imaging data. After data matching, a subset of 81 subjects (an average age of 38.01 ± 13.37 years) with both modalities was selected for this study. In terms of phyllodes tumor class, there were 65 benign, 10 borderline, and 6 malignant subjects. For this study, we merged the borderline and malignant categories to formulate a binary classification task.

B. Preprocessing

The BUS imaging data, originally in DICOM format, was converted to standard image format (PNG), and video files were decomposed into individual frames. Duplicate images were removed, and only frames containing tumors were retained. Since most BUS images included annotations along the image borders (e.g., probe position, frequency, and other metadata), we cropped the borders to exclude this information. Additionally, we converted RGB images to grayscale to ensure a consistent color profile across the dataset. The resulting image dataset consisted of 1,213 benign and 425 malignant images, yielding a class imbalance ratio of approximately 3:1.

The clinical dataset was then cleaned based on feature availability, retaining three numeric (age at diagnosis, BMI, and tumor size) and three categorical features (race, menopausal status, and tumor echogenicity). Categorical variables were processed using one-hot encoding, yielding a total of 10 clinical features.

C. Class-aware sampling

In highly imbalanced datasets, conventional random sampling often results in mini-batches dominated by the majority class, which can lead to biased model updates and poor generalization to minority classes. Class-aware sampling addresses this issue by decoupling the sampling process into two stages. First, a class is selected uniformly at random, ensuring equal sampling probability for each class regardless of its prevalence in the dataset. Second, a sample is drawn uniformly from within the selected class. By repeating this process, the constructed mini-batches contain a more equitable distribution of classes over time. This approach has effectively improved the training dynamics of deep learning models on long-tailed and imbalanced datasets [11]–[13].

D. Multimodal Deep Learning Framework

In this work, we adapted a multimodal deep learning framework to integrate both ultrasound image and clinical data as inputs. Our multimodal architecture consists of two parallel branches as illustrated in Figure 1.

The imaging branch is a convolutional neural network (CNN)-based image encoder to extract image embeddings from grayscale ultrasound images. In parallel, the clinical data, processed as a 10-dimensional feature vector, was passed through a multi-layer perceptron (MLP) to learn a compact representation of the clinical features and patient metadata.

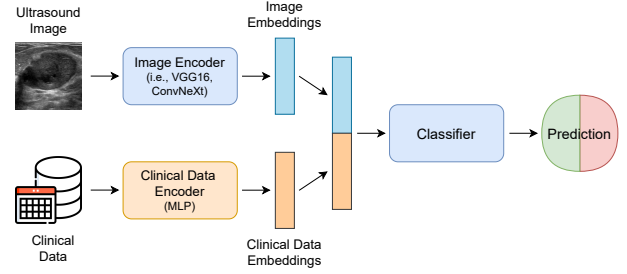


Fig. 1. Multimodal AI model overview.

Afterward, we used feature-level modality fusion by concatenating the feature embeddings. This enabled the classifier layers to learn complex cross-modal interactions that may be predictive of the target label but are not apparent in any single modality. Lastly, the combined feature vector was passed through a fusion module comprising additional dense layers, followed by a final softmax classifier.

This design enables the model to jointly reason over visual and tabular inputs, enhancing robustness and interpretability.

III. RESULTS

A. Experimental Setup

We performed subject-stratified 5-fold cross-validation to prevent data leakage across training and validation sets. Moreover, class-aware sampling was applied during training to address class imbalance. Ultrasound images were resized to 224×224 pixels and normalized to the $[0, 1]$ range. During training, we applied random horizontal flipping and slight rotation ($\pm 10^\circ$) as data augmentation. Each model was evaluated using average accuracy, F1-score, and its 95% confidence interval (CI) across folds. All experiments were conducted using an NVIDIA RTX A4000 GPU (16GB VRAM) and a system with 32GB RAM.

B. Evaluation of multimodal image encoders

We evaluated six image encoders—VGG16, ResNet18, ResNet50, EfficientNet-B7, CCT, and ConvNeXt—within the multimodal architecture. Table I summarizes the average accuracy, F1-score, and AUC-ROC over five subject-stratified cross-validation folds.

TABLE I
EVALUATION OF THE MULTIMODAL FRAMEWORK WITH DIFFERENT IMAGE ENCODERS (SORTED BY AUC-ROC)

Image Encoder	Mean Accuracy	Mean F1-Score	Mean AUC	95% CI (AUC)
ConvNeXt	0.9098	0.6720	0.9427	[0.8842, 1.0000]
CCT	0.9018	0.6683	0.9406	[0.8633, 1.0000]
ResNet18	0.9179	0.7294	0.9349	[0.8775, 0.9923]
ResNet50	0.9100	0.7065	0.9168	[0.8253, 1.0000]
EfficientNet-B7	0.8252	0.5473	0.8963	[0.8203, 0.9722]
VGG16	0.8885	0.6389	0.8886	[0.7376, 1.0000]

Among all models, **ConvNeXt** achieved the highest AUC-ROC of 0.9427, closely followed by CCT (0.9406) and ResNet18 (0.9349). **ResNet18** obtained the best average accuracy (0.9179) and F1-score (0.7294). In contrast, **EfficientNet-B7** and **VGG16** exhibited comparatively lower performance, particularly in F1-score (0.5473 and 0.6389, respectively), which may reflect their sensitivity to class imbalance or limited generalization on small datasets.

C. Attribution analysis

To improve the explainability of the model, we implemented Score-CAM to visualize the salient regions within ultrasound images to interpret the decision-making process of the model. Score-CAM creates visual explanations by passing activation maps through the model to get class scores. These scores are then used as weights to combine the maps into a final attribution [14]. Figure 2 illustrates examples of true positive, true negative, and misclassified cases using ConvNeXt as image encoder.

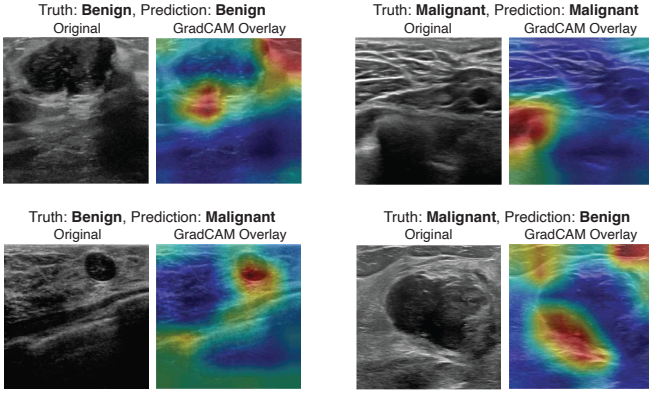


Fig. 2. Score-CAM attributes of the ConvNeXt image encoder benign and malignant cases. Warmer colors indicate regions contributing more strongly to the predicted class. Correctly predicted cases show focused attention on relevant tumor regions, whereas misclassified cases often exhibit diffuse or misplaced activations, suggesting visual ambiguity or model uncertainty.

For correctly predicted malignant cases, the image encoder focused on tumor regions and the surroundings with heterogeneous echotexture, while misclassified samples showed dispersed or ambiguous activation patterns. These insights suggest that visual cues alone are sometimes insufficient and further justify the use of multimodal reasoning.

D. Modality Ablation

We adopted a drop-based ablation approach to quantify the relative importance of each modality. For each sample, we computed the model’s predicted probability for the malignant class using all validation data across 5 folds. We repeated the process after zeroing out either the image or the clinical features. The magnitude of the change in probability is treated as the modality’s contribution. We normalized these changes to obtain relative contribution scores per sample. Figure 3 illustrates that BUS contributes 63% in the class prediction.

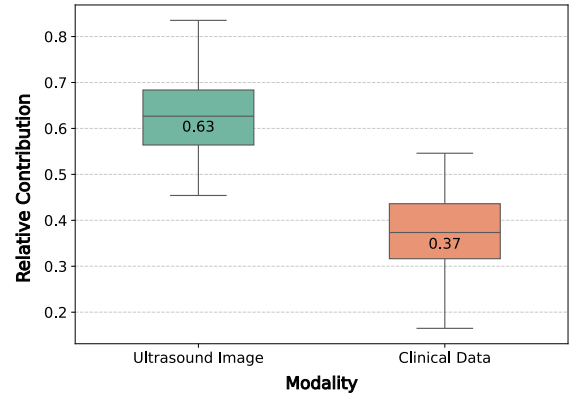


Fig. 3. Modality ablation analysis of our multimodal architecture.

E. Performance comparison between unimodal and multimodal approaches

We investigated the contribution of each modality by evaluating unimodal and multimodal models using our best-performing image encoder (ConvNeXt) and a multilayer perceptron (MLP) for clinical data. Table II summarizes the classification performance across different input configurations. The multimodal model achieved the best overall performance: accuracy of 0.9098, F1-score of 0.6720, and AUC of 0.9427. This highlights the benefit of combining heterogeneous data sources. The image-only ConvNeXt model also performed reasonably well (AUC = 0.8919), whereas the clinical data-only MLP showed substantially lower performance across all metrics, particularly the F1 score (0.33), indicating that clinical features alone may lack sufficient discriminative power. These results emphasize the effectiveness of multimodal fusion in improving diagnostic accuracy and robustness.

TABLE II
PERFORMANCE COMPARISON OF DIFFERENT INPUT MODALITIES

Modality	Accuracy	F1-Score	AUC	95% CI (AUC)
Only clinical data	0.8140	0.3300	0.7846	[0.6561, 0.9132]
Only BUS image	0.8906	0.6138	0.8919	[0.8259, 0.9578]
Multimodal	0.9098	0.6720	0.9427	[0.8842, 1.0000]

Figure 4 shows ROC curves for the two best-performing models, namely ConvNeXt and CCT, in both unimodal and multimodal configurations. The multimodal ConvNeXt model achieved the highest AUC (0.9427), followed closely by multimodal CCT (0.9406), both of which surpassed their unimodal counterparts. This reiterates the value of multimodal fusion, especially in cases where image features alone may be insufficient for confident classification.

IV. DISCUSSION

While unimodal models based solely on ultrasound imaging achieved reasonably strong performance, the multimodal approach consistently outperformed them across all key metrics. These improvements highlight the added value of integrating

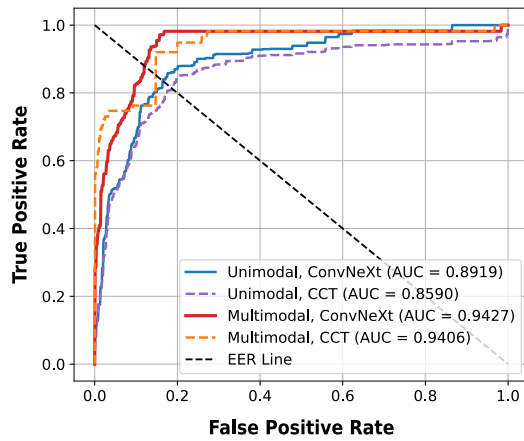


Fig. 4. ROC curves of the two best-performing models (VGG16 and ConvNeXt) with and without clinical data.

structured clinical data with imaging, enabling more accurate and robust classification, particularly in challenging borderline or malignant cases. Although the modality ablation study indicates a greater contribution from BUS images, the clinical data still plays a significant complementary role. This aligns with clinical practice, where radiologists incorporate both imaging findings and patient-specific risk factors in their diagnostic reasoning.

Moreover, Score-CAM visualization provides a foundation for clinical trust. Misclassified cases tended to exhibit weak or diffuse attention maps, indicating that the image encoder struggled with ambiguous visual patterns, which further justifies the use of auxiliary modalities.

Despite promising results, this study has a few limitations. The dataset is relatively small, especially for malignant and borderline cases, which limits the statistical strength of the findings. Although confidence intervals help assess variability, larger and more diverse multi-center datasets are needed before the clinical trial. Overall, this work shows that multimodal deep learning framework can improve phyllodes tumor diagnosis, even when working with small and imbalanced datasets, a common challenge in rare disease detection.

V. CONCLUSION

We proposed a multimodal deep learning framework that integrates ultrasound image features with structured clinical data for phyllodes tumor classification. Our proposed multimodal architecture consistently outperformed unimodal baselines across multiple image encoders, demonstrating improved diagnostic accuracy and robustness. This highlights the potential of this study to support clinical decision-making and reduce unnecessary surgical biopsies. One key challenge we encountered was the inherent class imbalance, with relatively few borderline and malignant cases. To address this, we applied class-aware sampling and subject-stratified cross-validation, which improved minority class representation during training.

Future work will aim to expand the dataset, incorporate radiologist annotations, and explore transformer-based encoders with attention mechanisms to enhance interpretability and performance. Prospective validation in real-world clinical settings will also be critical to assess the system's generalizability and its utility in guiding biopsy decisions.

REFERENCES

- [1] T. Soleimani, D. Euhus, O. Sogunro, L. Cope, M. Janjua, M. Vasigh, and L. K. Jacobs, "De-escalating indications for excision when breast core needle biopsy returns fibroepithelial lesion—not further characterized," *Breast Cancer Research and Treatment*, vol. 207, no. 3, pp. 561–568, 2024.
- [2] G. Lissidini, A. Mulè, A. Santoro, G. Papa, L. Nicosia, E. Cassano, A. A. Ashoor, P. Veronesi, L. Pantanowitz, J. L. Hornick *et al.*, "Malignant phyllodes tumor of the breast: a systematic review," *Pathologica*, vol. 114, no. 2, p. 111, 2022.
- [3] Y. Yan, Y. Liu, Y. Wang, T. Jiang, J. Xie, Y. Zhou, X. Liu, M. Yan, Q. Zheng, H. Xu *et al.*, "Hierarchical diagnosis of breast phyllodes tumors enabled by deep learning of ultrasound images: a retrospective multi-center study," *Cancer Imaging*, vol. 25, no. 1, pp. 1–13, 2025.
- [4] D. Mousa-Doust, C. K. Dingee, L. Chen, A. Bazzarelli, U. Kuusk, J.-S. Pao, R. Warburton, and E. C. McKeivitt, "Excision of breast fibroepithelial lesions: when is it still necessary?—a 10-year review of a regional centre," *Breast Cancer Research and Treatment*, vol. 194, no. 2, pp. 307–314, 2022.
- [5] Y. Yan, Y. Liu, J. Yao, L. Sui, C. Chen, T. Jiang, X. Liu, Y. Wang, D. Ou, J. Chen *et al.*, "Deep learning-assisted distinguishing breast phyllodes tumours from fibroadenomas based on ultrasound images: a diagnostic study," *British Journal of Radiology*, vol. 97, no. 1163, pp. 1816–1825, 2024.
- [6] A. Pfob, C. Sidey-Gibbons, R. G. Barr, V. Duda, Z. Alwafai, C. Balleyguier, D.-A. Clevert, S. Fastner, C. Gomez, M. Goncalo *et al.*, "The importance of multi-modal imaging and clinical information for humans and ai-based algorithms to classify breast masses (inspired 003): an international, multicenter analysis," *European radiology*, vol. 32, no. 6, pp. 4101–4115, 2022.
- [7] C. Ben Rabah, A. Sattar, A. Ibrahim, and A. Serag, "A multimodal deep learning model for the classification of breast cancer subtypes," *Diagnostics*, vol. 15, no. 8, p. 995, 2025.
- [8] S. Muhtadi and C. M. Gallippi, "Breast tumor diagnosis via multimodal deep learning using ultrasound b-mode and nakagami images," *Journal of Medical Imaging*, vol. 12, no. S2, pp. S22 009–S22 009, 2025.
- [9] J. Chen, T. Pan, Z. Zhu, L. Liu, N. Zhao, X. Feng, W. Zhang, Y. Wu, C. Cai, X. Luo *et al.*, "A deep learning-based multimodal medical imaging model for breast cancer screening," *Scientific Reports*, vol. 15, no. 1, p. 14696, 2025.
- [10] P. Xu, J. Zhao, M. Wan, Q. Song, Q. Su, and D. Wang, "Classification of multi-feature fusion ultrasound images of breast tumor within category 4 using convolutional neural networks," *Medical Physics*, vol. 51, no. 6, pp. 4243–4257, 2024.
- [11] L. Shen, Z. Lin, and Q. Huang, "Relay backpropagation for effective learning of deep convolutional neural networks," in *Computer Vision—ECCV 2016: 14th European Conference, Amsterdam, The Netherlands, October 11–14, 2016, Proceedings, Part VII 14*. Springer, 2016, pp. 467–482.
- [12] D. Scholz, A. C. Erdur, J. A. Buchner, J. C. Peeken, D. Rueckert, and B. Wiestler, "Imbalance-aware loss functions improve medical image classification," *Medical imaging with deep learning*, pp. 1341–1356, 2024.
- [13] M. Varaganti, A. Vankayalapati, N. Awad, G. R. Dion, and L. J. Brattain, "T2id-cas: Diffusion model and class aware sampling to mitigate class imbalance in neck ultrasound anatomical landmark detection," *arXiv preprint arXiv:2504.21231*, 2025.
- [14] H. Wang, Z. Wang, M. Du, F. Yang, Z. Zhang, S. Ding, P. Mardziel, and X. Hu, "Score-cam: Score-weighted visual explanations for convolutional neural networks," in *Proceedings of the IEEE/CVF conference on computer vision and pattern recognition workshops*, 2020, pp. 24–25.